Islamic Azad University

Journal of
Optoelectronical Nanostructures

Summer 2021 / Vol. 6, No. 3

Research Paper

Electronic, Optical, and Thermoelectric Properties of $BaFe_{2-x}Zn_xAs_2$ (x=0,1,2) orthorhombic Polymorphs: DFT Study

Tahereh Niazkar[1], Gholamabbas Shams*[,1], Zahra Soltani[1]

[1] Department of Physics, Shiraz Branch, Islamic Azad University, Shiraz, Iran

Received: 27 Jun. 2021
Revised: 29 Jul. 2021
Accepted: 26 Aug. 2021
Published: 15 Sep. 2021

Use your device to scan and read the article online

Keywords:
$BaFe_{2-x}Zn_xAs_2$, DFT, Thermoelectric Properties

Abstract:

Based on the calculations of density functional theory and Generalized Gradient approximation (GGA), mechanical, electronic, optical and thermoelectric properti $BaFe_{2-x}Zn_xAs_2$ (x=0,1,2) have been investigated in orthorhombic phase. For all three $BaFe_{2-x}Zn_xAs_2$ (x=0,1,2), the energy curves have an equilibrium point in terms of their volume. For x=1 and x=2, the bonds take on an ionic shape. Electronic calculations show that by applying the modified Becke-Johonsom (mBJ) approximation, the x=2 compound is converted to a p-type semiconductor with a gap of 0.11 eV. However, magnetic behavior can be seen for the other two impurities. At x=2, the band structure illustrates a direct gap. Optical diagrams display that the parts of the dielectric function exhibit strong metallic behavior for impurities x=0, 1, and also an optical gap can be detected. Moreover, the Seebeck coefficient provides that a good stability is observed in its behavior at room temperature onwards to reach the saturation limit of 200 μvK-1. Additionally, the figure of merit reaches a saturation limit in the range of 0.6 to 0.7 at this temperature range.

Citation: Niazkar T. Shams Gh A. Soltani Z. Electronic, Optical, and Thermoelectric Properties of $BaFe_{2-x}Zn_xAs_2$ (x=0,1,2) orthorhombic Polymorphs: DFT Study. **Journal of Optoelectronical Nanostructures. 2021; 6 (3): 93-116. DOI:** 10.30495/JOPN.2021.28945.1237

***Corresponding author:** Gholamabbas Shams
Address: Department of Physics, Shiraz Branch, Islamic Azad University, Shiraz, Iran. **Tell:** +989175380576 **Email:** shams_physics@yahoo.com

1. INTRODUCTION

Since the discovery of high temperature (Tc) superconductivity in layered copper oxides, extensive efforts have been made to detect higher Tc superconductivity. However, Tc above 40K can only be obtained in copper oxide superconductors. The highest reported Tc value for non-copper bulk superconductivity is in MgB2 [1]. The TC is about 40K closer to or greater than the theoretical value predicted by BCS theory [2].

Recently, a new class of high temperature superconductors has been discovered based on iron-arsenic layered structures [3]. The 122 triple phases, with over 600 combinations, form a large family of materials with exciting physical properties. Recently, applications for spintronics from 122 phases have been proposed as a promising platform to search for dilute magnetic semiconductors, for example the $BaZn_2As_2$ semiconductor [4-9]. Superconductivity is one of the most interesting and attractive phenomena in condensed matter physics. Below the transition temperature, Tc, the electrical resistance of these materials is zero, and they also show full diamagnetic properties. This macroscopic phenomenon has its roots in the quantum mechanics of electrons. The formation of electron pairs by a small absorption interaction between them (this pair of electrons is called the Cooper pair). In conventional superconductors, this coupling is due to electron-phonon interaction, and this process has been understood using the microscopic model by three scientists, Bardin, Cooper, and Schriffer, or BCS for short [1]. It has been theoretically shown that for superconductivity due to electron pair formation caused by electron-phonon interaction, a superconductivity transition temperature higher than 40 K is not possible. In any case, with the advent of copper oxide in 1986, this theoretical limit for the transition temperature was broken. For example, a transition temperature of 133 K is achieved in mercury-based copper oxide superconductors. In addition to these compounds, various materials later called unconventional superconductors or high temperature superconductors were subsequently made. Superconductivity in these materials cannot be described by the mechanism of electron-phonon interaction. Cuprate superconductors have complex phase diagrams. For example, in copper oxide superconductors (Cuprates), several complex phase ranges are seen. The repulsion between electrons at the lattice site, for example the opaque insulation phase in doper-free compounds, or the complex quasi-gap phenomenon, can be due to the effects of strong correlation between electrons. Therefore, the discovery of high temperature superconductors with a state (phase) diagram can help more easily to understand

the physics of the problem. The efforts on this route led to fabrication of the new family of superconductors by a Japanese group led by Hosunu. These compounds have an iron element. Therefore, this new family is called iron-based superconductors. One of these materials is the LaFeO1-xFx combination formed by FeP and LaO layers [10]. The transition temperature of these compounds is 5 K. Subsequently, the same group of materials LaFeO1-xFx is made by substituting AS instead of P, and the transition temperature increased to 26K [11-14]. This discovery attracted a lot of attention because these compounds could have a good candidate for breaking the record temperature of 133 K in mercury-based Cuprates. In addition, these materials can provide a good ground for finding superconductor microscopic theory, i.e. the understanding of the Cooper pair mechanisms in unconventional superconductors because iron-based superconductors have similar properties with Cuprates. Including that electron or hole doping and applying chemical or mechanical pressure can cause favorable conditions for superconductivity phases. Moreover, this group of superconductors has a layered structure and anisotropy. An interesting thing about iron-based superconductors is that unlike Cuprate superconductors that any changes in copper oxide layers leads to suppressing superconductivity, in this family, superconductivity is maintained by creating changes in the Fe-As layers such as contamination with different elements instead of iron [13]. Several questions, including the role of magnetism, contaminations, and crystalline structure in superconductor properties in these materials are still unanswered. Another most well-known combination of this family is $BaFe_2As_2$ so that experimental and theoretical studies have been done on this compound. In this research, the effects of substituting the Zn atom instead of the iron element in the $BaFe_2As_2$ compound will be discussed.

2. COMPUTATIONAL DETAILS

The first principles calculations are carried out using the density functional theory (DFT) [15], in which the many-body interaction of electrons and nucleuses, the Kohn–Sham equations, are reduced to an electron equation [16]. Solving of the Kohn–Sham equations is done using the full-potential linearized augmented plane-wave (FP-LAPW) method [17], which is used in the Wien2K package [18]. Replacing the correlation potential is calculated using Perdew-Burke-Ernzerhof parametric in generalized gradient approximation (PBE-GGA) [19]. The spin-orbit calculations are performed for both up and down spin

modes. The wave functions in the cutoff area spread in plane waves with cutoff RKmax=8.0. The radius of the muffin-tin (RMT) is considered 2.0 a.u. for all atoms. The number of lattice points, K, in the first Brillouin zone is 8×20×8 in the irreducible Brillouin zone. In the following, the calculations of static mechanical stability (volume-energy curve), and electronic properties are done by Wien2K software. At the end, BoltzTraP software is used to investigate the thermoelectric characteristics of these compounds..

3. RESULTS AND DISCUSSION

A. Structural Properties

In Figure (1) Panels (a) to (c), Orthorhombic structure of the $BaFe_{2-x}Zn_xAs_2$ compound has been drawn which by entering the impurities of Zn instead of the Fe atom and the change of Fe share, three different structures of this compound are made. As it is known, the Fe atom belongs to transition metals which have metallic and magnetic properties. Furthermore, the Zn metal does not have magnetic properties with the orbital structure of (Zn = [Ar] $4s^2 3d^{10}$).

On the other hand, substituting the Zn atom instead of the iron atom seems reasonable according to this fact that the Zn atomic number is close to the Fe atomic number. For these three structures mentioned in Figure (1), in the first step, it must be shown that there is stability which have been discussed from two perspectives; first, a search for the equilibrium volume and the ground state point, and then, comparing its cohesive energy. In this regard, changes in the total energy of a crystal relative to volume changes, based on the Murnaghan equation, give valuable information about mechanical stability, such as the equilibrium volume from which lattice constants are extracted, bulk module and derivative bulk module.

(a) $BaFe_{2-x}Zn_xAs_2(x=0)$

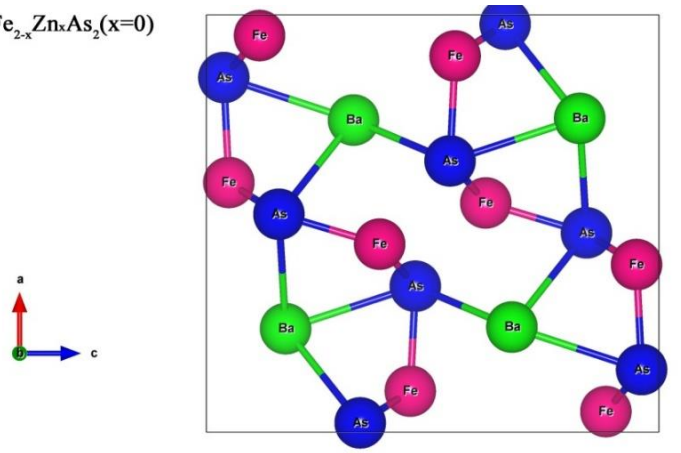

(b) $BaFe_{2-x}Zn_xAs_2(x=1)$

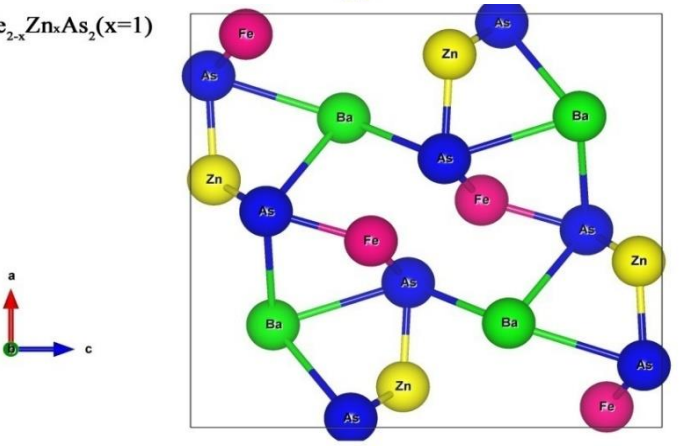

(c) $BaFe_{2-x}Zn_xAs_2(x=2)$

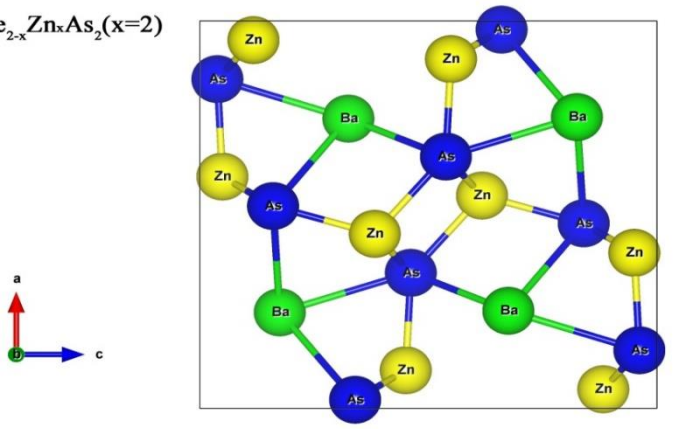

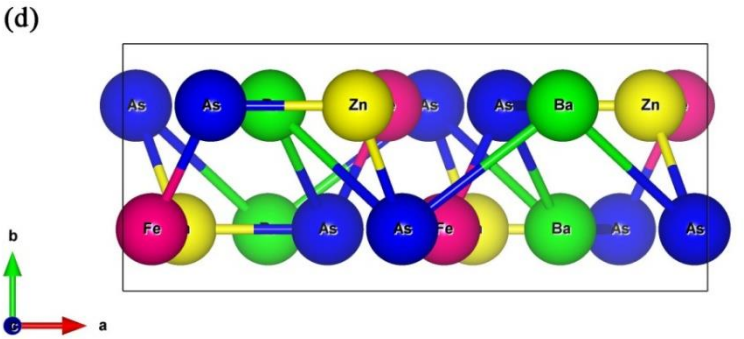

Fig. 1. The crystal structure of for different values of x, (a) x=0, (b) x=1, (c) x=2 in two axis of a and c , (d) x=2 in two axis of a and b

Figure (2) shows the energy curves in terms of volume (E-V) of these three compounds. The common point in all three diagrams is their parabolic behavior. The presence of a minim point indicates the equilibrium volume, where the energy of its unit cell is at its lowest value, so it can be said that all three structures are mechanically stable. The results of these calculations are listed in Table (1).Comparing these three graphs, it can be seen that the diagram in panel (a) is more symmetrical than panel (b) and (c), meaning that this combination shows the same reactions to the pressure under stress or strain. In the panel (b) and (c), the slope of the curve in the left side of the equilibrium point is steeper, indicating that more pressure must be applied to the crystal under stress to cause a volume change. From Table (1), it is seen that the minimum point energy for $BaFe_{2-x}Zn_xAs_2$ (x=2) compound has the lowest value while the) $BaFe_{2-x}Zn_xAs_2$ (x = 0) compound has the highest value. Therefore, it can be said that this system is most interested in being transferred to the phase state of) $BaFe_{2-x}Zn_xAs_2$ (x = 2).

If we want to synthesize this compound in the laboratory, it is more inclined to $BaFe_{2-x}Zn_xAs_2$ (x=2) state. Table (1) also has information such as B, B'. Looking at the bulk modulus of these three compounds, it can be observed that the crystal stiffness are relatively large numbers [20] which is larger than glass and smaller than Steels. This shows that this compounds are expected to be capable of industrial applications. The bulk module derivative is a dimensionless quantity, containing important information. This parameter reveals the pressure change of the bulk modulus of $BaFe_{2-x}Zn_xAs_2$ (x= 0, 1, 2) that the type of interatomic bonds in them is ionic, so this is another proof of the strength of the electrical bonds between these atoms.

 DOI: 10.30495/JOPN.2021.28945.1237

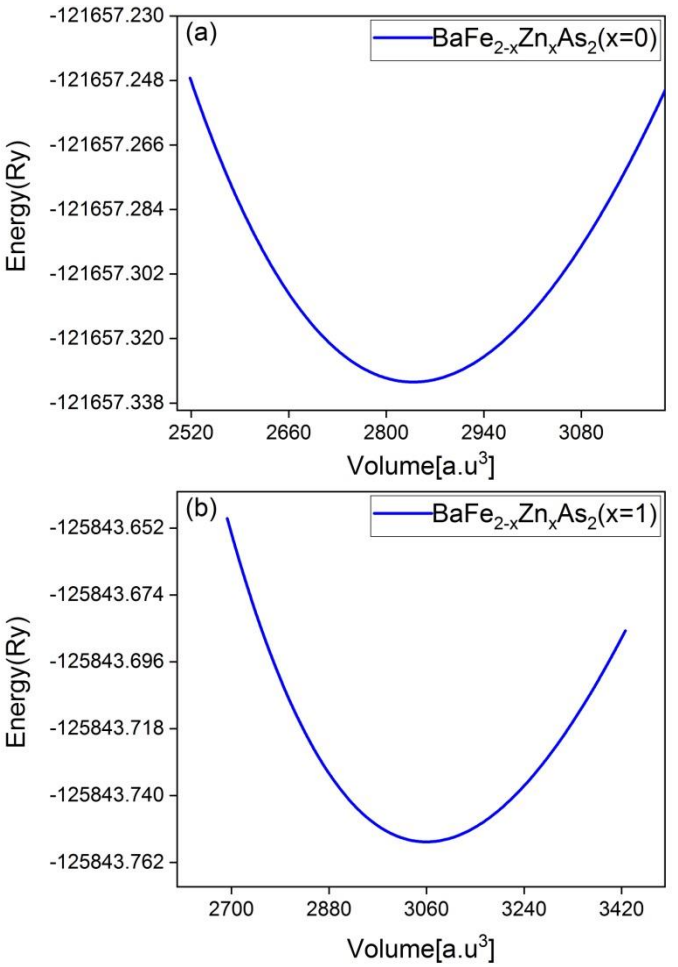

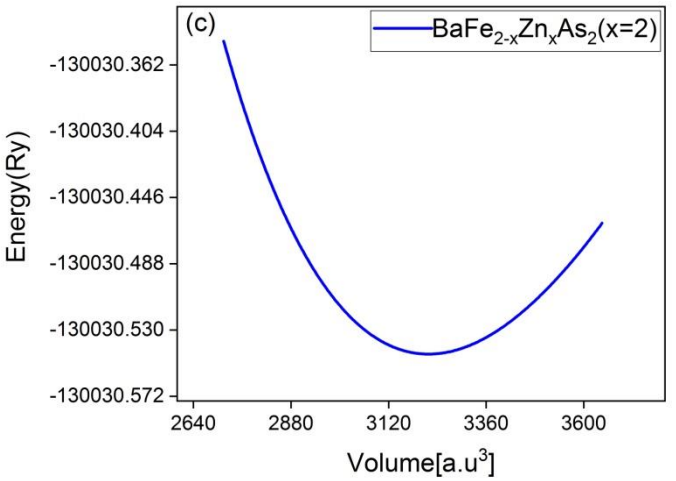

Fig. 2. The energy-volume of $BaFe_{2-x}Zn_xAs_2$ for different values of x. (a) x=0, (b) x=1, (c) x=2

TABLE 1
The lattice parameters (a, b, c), equilibrium volume, bulk modulus, derivative buk modulus B', energy in ground state point, total magnetic moment (M_{tot}).

paramtere	a(bohr)	b(bohr)	c(bohr)	Volume[a.u3]	B(Gpa)	B'	Energy(Ry)	M_{tot}
$BaFe_{2-x}Zn_xAs2(x=0)$	18.3560	7.7646	19.9163	2838.6187	59.8789	2.5524	-121657.3321	20.710
$BaFe_{2-x}Zn_xAs2(x=1)$	18.8655	7.9801	20.4690	3059.7498	56.6918	4.2769	-125843.7552	12.4782
$BaFe_{2-x}Zn_xAs2(x=2)$	19.1847	8.1151	20.8154	3217.7020	54.1376	4.5795	-130030.5453	0.00

TABLE 2
Atomic position of the $BaFe_{2-x}Zn_xAs_2$ (x=0,1,2) compounds.

Position	x	y	z
Ba	0.2480	0.25	0.820
Fe_1,Zn_1	0.0494	0.25	0.1173
Fe_2,Zn_2	0.0984	0.25	0.549
As_1	0.4777	0.25	0.1602
As_2	0.3499	0.25	0.5384

B. Electronic Properties

Electron density is very important in electronic processes, especially in transport phenomena. Using it for the electrons of a crystal, in addition to calculating the amount of band gap, it is possible to correctly determine the orbital contribution of each of the atoms participating in the composition. The calculations are performed considering spin using mBJ and GGA approximations.

In Figure (3) panels of (a), (b) and (c), total DOS and partial DOS (PDOS) are observed for the $BaFe_{2-x}Zn_xAs_2$ compound for x = 0,1, and 2 in two spins of up and down. For the impurities of x=0 and x=1, a large magnetic anisotropy can be witnessed at their Fermi level, and these two compounds have half-metallic behavior with spin polarization of %47 and %46 for x=0 and x=1, respectively. However, in the impurity x=2 in panel (c) with GGA approximation, nonmagnetic semiconductor behavior is observed with 0.0eV gap. Furthermore, by applying the mBJ approximation, the electronic states of the conduction region shift to higher energies. As a result, the semiconductor gap has increased to 0.11eV. It can be seen that a very important points in this impurity are that firstly, its semiconductor properties are p-type, and secondly, the electronic states in the conduction and valence regions are completely continuous so that there is not any gap in these two regions. This indicates the high transport capacity of electrons and holes in this impurity. Nevertheless, in two impurities of x=0 and x=1, energy gaps are seen in the valence region and a tendency to decrease in the conduction region. This causes the conductivity in these two compounds to be dependent on applying magnetic field. In panel (d), PDOS of the effective orbitals are shown. Here, it is see that the highest effect in panels (d) and (e) for magnetizing these two compounds at the Fermi level belongs to the d orbitals of the iron atoms. Additionally, for the x=0, below the Fermi region, d orbitals of the Ba atom plays the same role, but in panel (f), it is observed that the share of the Fe atom is lost. As a result, the compound exhibits a completely non-magnetic behavior. In the valence region, the highest share belongs to the p orbitals of the As atom, followed by the other orbitals shown in Figure. Despite that, in the conduction region, the highest share belongs to the d orbitals of the Ba atom and then the p orbitals of the As atom. Consequently, the p orbitals of the As atom play an important role in the hole transport in this type of semiconductors (p-type semiconductors) and in this compound. The overlap of these diagrams demonstrates the establishment of the p-d and s-p bonds.

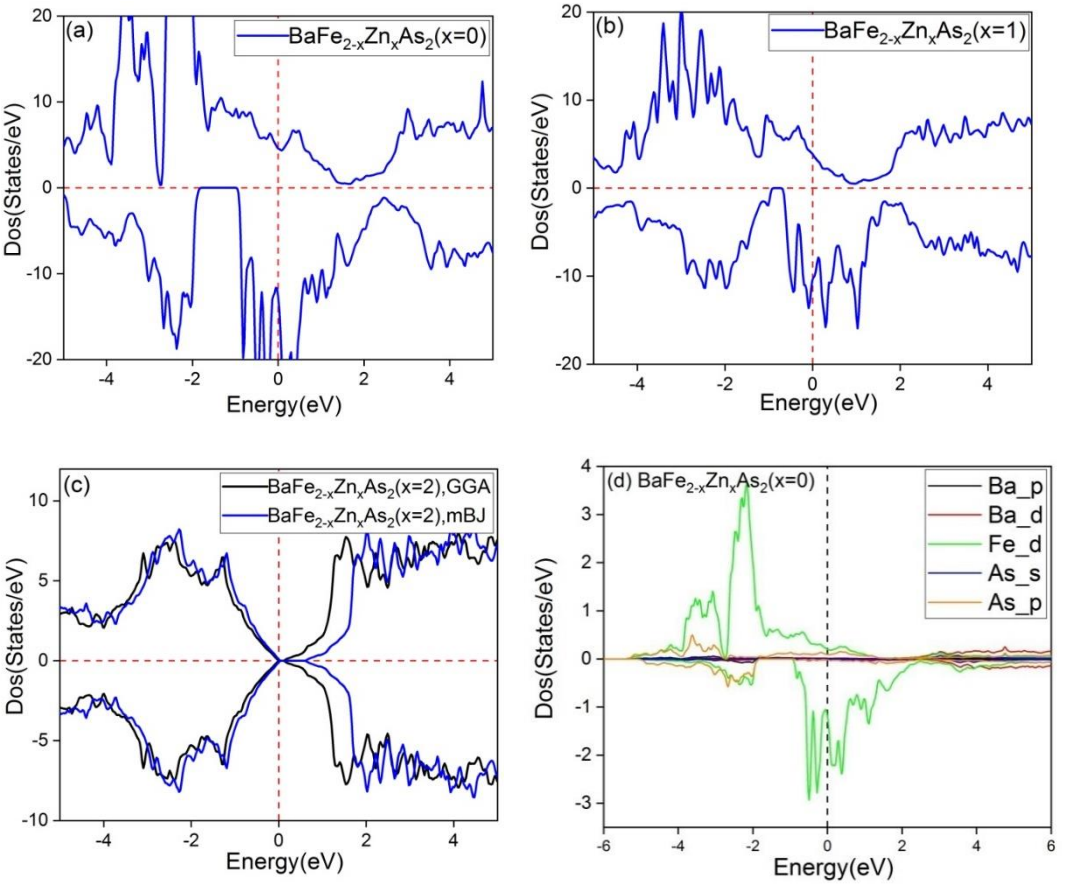
(a)
BaFe2-xZnxAs2(x=0)
Dos(States/eV)
Energy(eV)
(b)
BaFe2-xZnxAs2(x=1)
Dos(States/eV)
Energy(eV)
(c)
BaFe2-xZnxAs2(x=2),GGA
BaFe2-xZnxAs2(x=2),mBJ
Dos(States/eV)
Energy(eV)
(d) BaFe2-xZnxAs2(x=0)
Ba_p
Ba_d
Fe_d
As_s
As_p
Dos(States/eV)
Energy(eV)

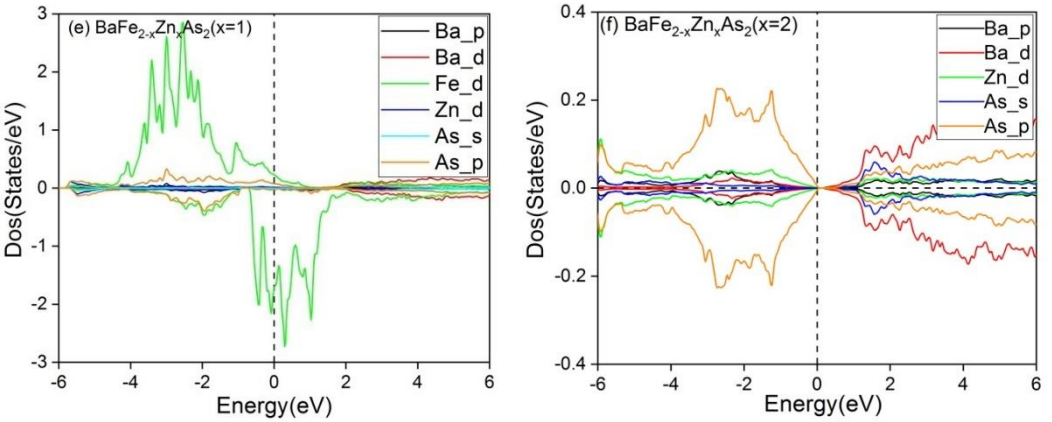

Fig. 3. The total DOS of) BaFe $_{2-x}$Zn$_x$As$_2$compounds, (a) x=0 (b) x=1,(c) (x=2).The partial DOS of BaFe2-xZnxAs compounds (d) x=0, (e) x=1, (f) x=2

In free atoms, there are separate energy levels, but in solids, the available energies are so close together that they form a band. The energy of the electrons inside the crystals is arranged in energy bands. A band gap is defined as the difference between the highest occupied band (valence band) and the lowest unoccupied band (conduction band). The band gap is important because it determines the type of material The band gap is one of the most useful aspects of the band structure, greatly affecting the optical, electronic and thermoelectric properties .In Figure (4), the band structure diagrams of these three compounds are in very good agreement with the DOS diagrams, and panels of (a) and (b) are depicted for x=0. It is quite clear that in the up spin, the electronic levels are intertwined from the -5 eV range upwards by applying a magnetic field, and a strong metallic behavior is observed at the Fermi level due to the gradient of the levels. By changing the direction of the magnetic field, a gap below the Fermi level emerges, and the energy levels at the Fermi level are accumulating. The same thing happens at x=1 as the highest conductivity occurs at R→Γ and at M→Γ. At x=2, a direct band gap of about zero is detected for GGA and another direct band gap of about 0.11eV for mBJ. It is clear observed that in this model, in addition to the Fermi region gap, three other gaps occur in the valence region. Besides, the slope of the levels declines at lower energies while the slope and gradient of the levels are increased in the Fermi range of the conduction region. In x=2 compared to x=0, the density of the levels at the Fermi level is reduced owing to the replacing the iron atom. The existence of this direct band gap is declaring a good optical and thermoelectric applications.

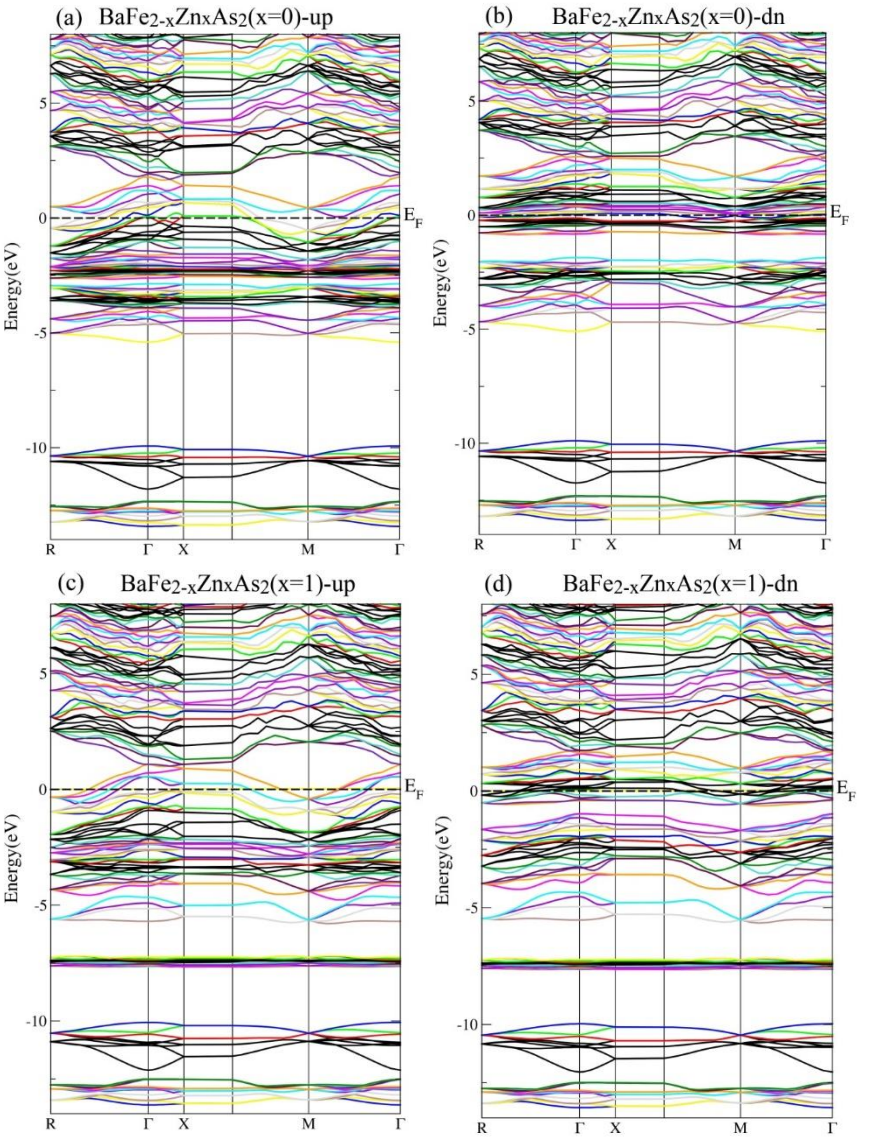
(a) BaFe2-xZnxAs2(x=0)-up
(b) BaFe2-xZnxAs2(x=0)-dn
(c) BaFe2-xZnxAs2(x=1)-up
(d) BaFe2-xZnxAs2(x=1)-dn
Energy(eV)
E_F
R
Γ
X
M
Γ

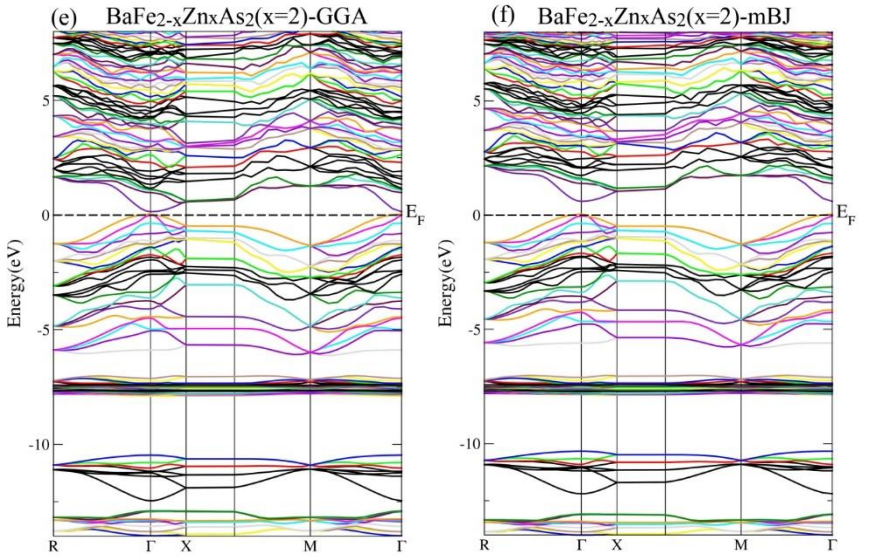

Fig. 4 The bandstructure of the BaFe $_{2-x}Zn_xAs_2$ compound .(a)x=0 up ,(b)x=1 dn,(c) x=1 up, (d)x=1 dn, (e)x=2 up , (f) x=2 dn

C. Optical Properties

The dielectric functionε(ω, K) using optical spectroscopy is very useful in determining the overall band structure of a crystal. In order to investigate the interaction of photons with matter and to obtain the optical properties, the dielectric function of the material is investigated. In fact, this function is the crystal response to the electromagnetic field. The dielectric function is a complex function in the form of ε(ω)=ε1(ω)+iε2(ω). By having the imaginary part for all frequencies, the real part can be obtained from the Kramers-Kronig transformation [21]:

$$\mathrm{Re}\,\varepsilon^{-1}(q,\omega) = 1 + P\int_{-\infty}^{+\infty} \frac{\mathrm{Im}\,\varepsilon^{-1}(q,\xi)}{\pi}\frac{d\xi}{\xi-\omega}\,, \tag{1}$$

$$\mathrm{Im}\,\varepsilon^{-1}(q,\omega) = -P\int_{-\infty}^{+\infty} \frac{\left[\mathrm{Re}\,\varepsilon^{-1}(q,\xi)-1\right]}{\pi}\frac{d\xi}{\xi-\omega}\,, \tag{2}$$

This function has two intraband and interband transitions. The intraband transition is due to excitation of volumetric Plasmons (Collective oscillations of

free electrons with a longitudinal wave or compressional-wave, which are induced in metals by an electron beam or a charged-particle, that is excited also in semiconductors and insulators) [31, 32] and interband transition is owing to excitation at the absorption edges. The value of the dielectric function is approximately zero at very low energies.

Figure (5) illustrates the diagrams of the real and imaginary parts of ε for the incident light directions of x and z. In panel (a) and (b), the real parts of the dielectric function are plotted for two impurities of x=0 and x=1 for the two directions of x and z. The generalities of these two figure are so similar that the static values of the real-ε tend to infinity, indicating a very strong metallic behavior. However, in the visible to UV regions, they have positive values with a peak, so that their main peak is at the visible edge, occurring for x=1, while their maximum values experience a Blue shift for x=0. In panel (c), the static values for the real-ε for both directions are positive and the finite values in which the tendency for semiconductor behavior can be detected. Here, the peaks of the dielectric function occur in the range from 2 to 3 eV in both the x and z directions, but as the energy of the incident photon increases, the value decreases so that it becomes zero and less than zero in the range of 4.5 eV onwards. In addition, in the range from 4.5 to 12 eV, this compound exhibits a negative response, so the application of this compound can mostly be defined in the visible region. In panels of (d), (e) and (f), the imaginary part of the dielectric function is plotted in the two mentioned directions, so that the same behavior can be observed for the two impurity states of x=0 and x=1.The peaks in this diagram represent interband and intraband transitions. It is observed that due to the metallic properties of these two compounds, their static values tend to infinity and the transitions are predominantly of the intraband type, such that by increasing the incident photon energy up to 2 eV, a sharp decrease is detected in these graphs. At x=1 in both x and z directions, there is a peak in the visible region, and smaller peaks are experienced in the range of 4 to 5 eV. Then, the graphs shift to smaller values, demonstrating transparent behavior at energies of 8 eV. In panel (f), it is reported that the physical properties are quite different, representing a semiconductor behavior as a 1 eV optical gap can be witnessed. After that, large peaks are seen from 3.5 to 4.5 eV in both x and z directions. By increasing the incident photon energy from 8 eV onwards, the values of this graph become very small, so it can be said that most of transitions are the interband type, occurring in the range of 2 to 6 eV.

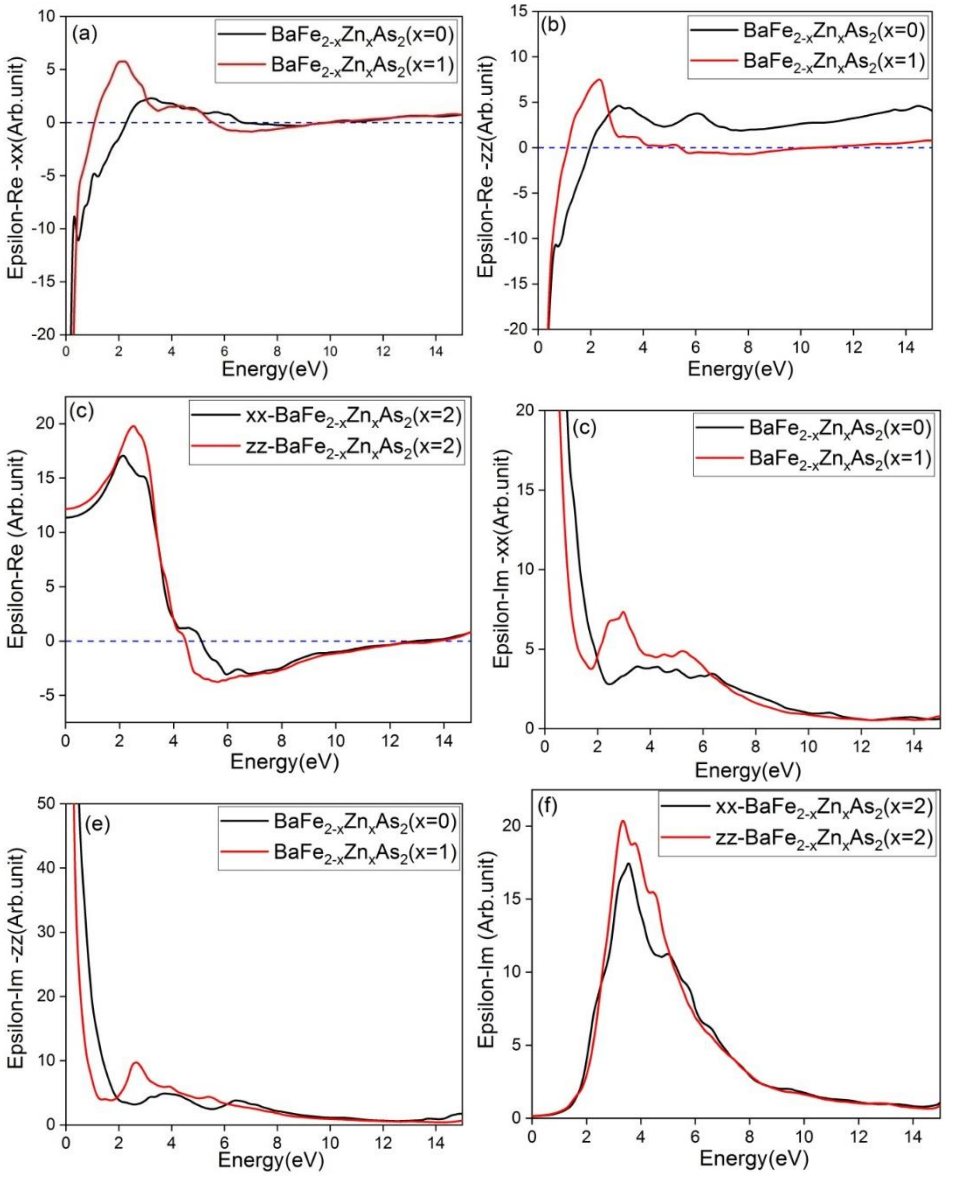

Fig. 5. (a) and (b) the real and imaginary coefficients of $BaFe_{2-x}Zn_xAs_2$ (x=0,1) compounds. (c) the static values for the real-ε for both directions x,z in x=2. (d), (e) and (f), the imaginary part of the dielectric function $BaFe_{2-x}Zn_xAs_2$ (x=0,1,2)

In Figure (6), the energy loss function spectrum is plotted. In panel (a), it can be seen for the x-axis direction for the x=0 and x=1 compounds that a peak is observed in the region of 1.5 eV for x=1 while there is a peak in the region of 2.3 eV for x=0. Most of the peaks occur from 8 eV onwards. According to the zero value of the real-ε at this region energy in the either x or z directions, these peaks in the x direction represent Plasmon oscillations. In the z-axis direction, the maximum energy loss occurs in all energy ranges for x=1, and the loss is very small for x=0. As it is expected, because of the semiconductor nature of the impurity x=2, the energy loss function spectra of this impurity are zero and very small in the IR and visible regions. Moreover, the major loss occurs at the 10 eV and onwards, so Plasmon oscillations occurred here are owing to the zero value of the real-εat this energy (12 eV).

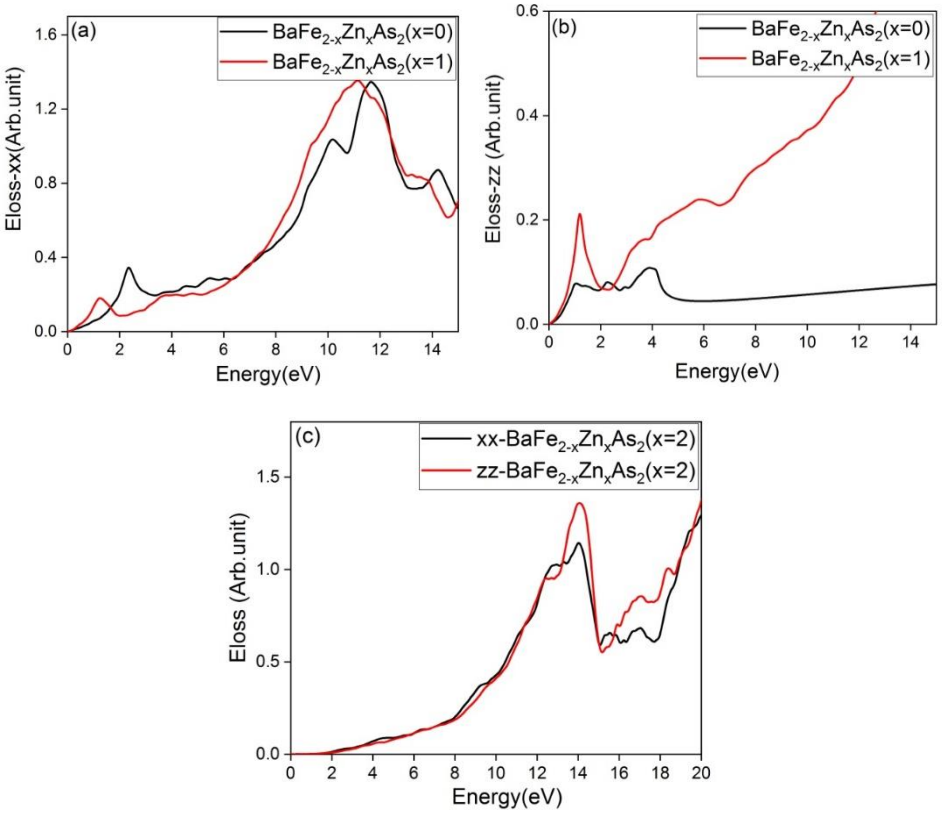

Fig. 6 The ELOSS of $BaFe_{2-x}Zn_xAs_2$ compounds. .(a) x=0 (b) x=1 (c) x=2

D. Thermoelectric Properties

Nowadays, obtaining suitable thermoelectric (TE) materials has become one of the most extensive fields of research [32-36]. TE materials are materials that can generate voltage using temperature differences, or, conversely, generate temperature gradients using potential differences, which are used in two advanced industries: power generators and cooling. Modern solid-state thermoelectric devices are a special solution to the challenge of using large-scale or small-scale heat dissipation. In fact, peripherals are solids used for heat management and engineering, so electrons and holes act as liquids in semiconductor materials. The goal of engineering these materials in energy conversion programs is to maximize the electrical power [22].

The thermoelectric efficiency of the material can be measured by calculating the dimensionless figure of merit, ZT, as well as the power factor which can be calculated using the following formula.

$$ZT = {S^2\sigma T}/{K} \quad (3)$$

$$PF = S^2\sigma \quad (4)$$

Where T is the absolute temperature, S is the thermopower coefficient, σ is the electrical conductivity and K is the thermal conductivity value including the lattice and electron contributions (K=Kel+Klatt) [23-26].

In Figure (7) panels of (a) to (e), thermoelectric diagrams of thermoelectric parameters of the $BaFe_{2-x}Zn_xAs_2$ (x=2) compound are depicted. For the x=2 structure, which is a p-type semiconductor with a direct band gap, is drawn under temperature. It is observed that this coefficient is at its lowest value at a temperature of 50 K, and it increases to 200 K with a steep slope. From the room temperature onwards, it reaches 200 μvk-1, and it reaches its saturation number at this value. It can be seen that the magnitude of this coefficient at room temperature is comparable and even larger than many other theoretical and experimental compounds [27-30].It is also clear that the sign of this coefficient is positive in all temperature ranges, providing that this compound has a p-type semiconductor behavior. At the room temperature, due to a temperature gradient difference, emerging a great potential can be witnessed in this compound. The electrical conductivity of this compound in panel (b) demonstrates that the conductivity increases with a relatively steep slope by increasing temperature,

and given that two electron states has touched the Fermi level, the conductivity is not zero at 50 K. Panel (c) shows the thermal conductivity due to the electron contribution. It is observed that there is a thermal conductivity gap up to the range of 100 K, and increasing temperature, this parameter has increased with a steep parabolic slope afterwards. Therefore, this compound can behave like a heat switch by changing the temperature. In panel (d), the dimensionless figure of merit is drawn under temperature. The efficiency is low at low temperatures, but it reaches a saturation limit in the range of 0.7 after 200 K, indicating that the compound has a high thermoelectric quality at the room temperature and above. In panel (e), there is the power factor (PF) graph, the value of which is zero at 50 K and increases with a sharp slope by increasing temperature. At room temperatures onwards, the value of this parameter is an acceptable value compared to other compounds [24], so it can be suggested that this compound can be used as power generator compounds.

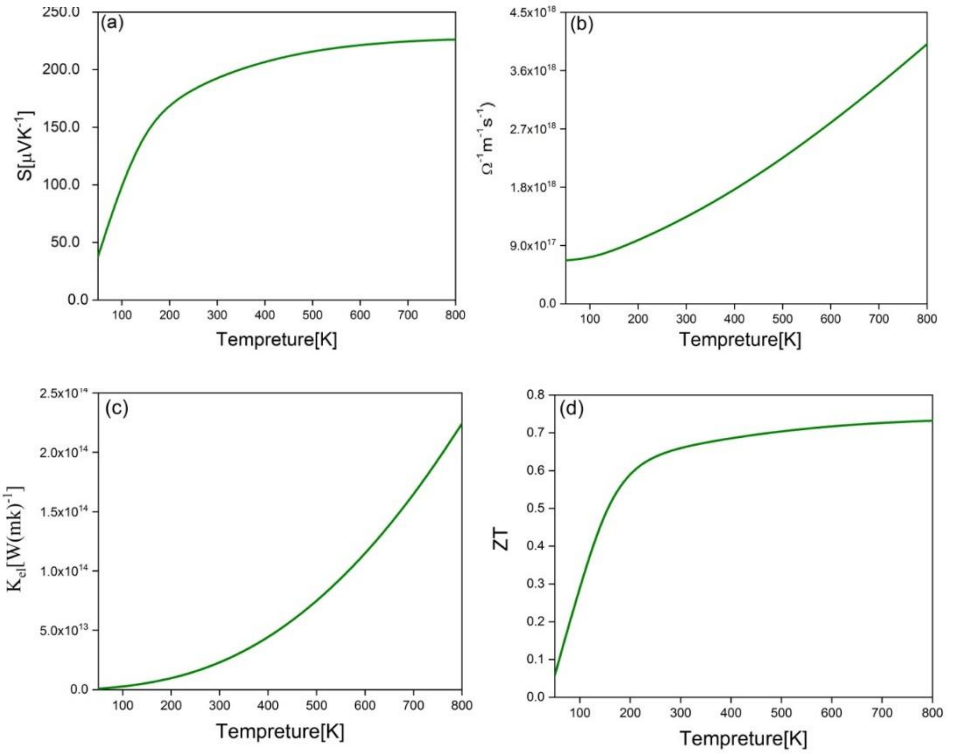

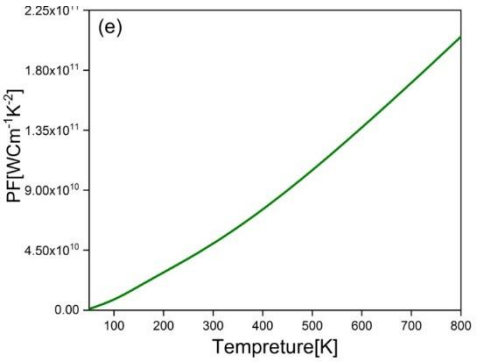

Fig. 7. Thermoelectric diagrams of thermoelectric parameters of $BaFe_{2-x}Zn_xAs_2$, x=2 (a) in the room temperature. (b) in 50 K, (c) in 100 K, (d) in 200 K
(e) the graph of power factor (PF)

4. CONCLUSION

Based on density functional theory and the full-potential linearized augmented-plane wave (FP-LAPW) method, mechanical, electronic, optical, and thermoelectric properties of (x=0,1,2) have been examined under the effect of 3 different percentage of impurity. The result of the band structure reveals that all three structures have mechanical stability and equilibrium volume, and their crystalline stiffness is higher than glass. The results of the bulk modulus derivative demonstrate that the bond type is covalent in the x=0 impurity state and ionic in the other two impurities. Furthermore, the magnetic moment is zero at x=2 while it is 20.71 and 12.47 at x=0 and x=1, respectively. The DOS and band structure diagrams illustrate that the structures exhibit half-metallic behavior with spin polarization at the Fermi level for x=0 and x=1, but the p-type semiconductor behavior is witnessed at x=2 with a direct gap of 0.11 eV in the mBJ approximation and 0.0 eV in the GGA approximation. The diagrams of the optical section prove the findings of the electronic section, so that the static values of Real-ξ tend to infinity at x=1, but they show a value around 12 at x=2. In addition, an optical gap is detected in impurity x=2. Due to the small gap that existed in impurity x=2, suitable thermoelectric properties is obtained from it, so that this compound has good thermoelectric stability above the room temperature and the value of its Seebeck coefficient is greater than 200μvk-1. Besides, at high temperatures, the figure of merit is in the range of 0.7, indicating the acceptable thermoelectric efficiency of this compound. The power factor of this compound provides that it can be used for power generator purposes.

REFERENCES

[1] J. Nagamatsu, N. Nakagawa, T. Muranaka, Y. Zenitani, J. Akimitsu , *Superconductivity at 39 K in magnesium diboride*. Nature Phys. Rev. 47, 777-780.410, (2001) 63-64.
Doi: https://www.doi.org/10.1038/35065039

[2] W.L. McMillan, *Transition Temperature of Strong-coupled superconductors*. Phys. Rev. 167, (1968) 331-344.
Doi: https://www.doi.org/10.1103/PhysRev.167.331

[3] Y. Kamihara, T. Watanabe, M. Hirano, H. J. Am. Hosono, *Iron-Based Layered Superconductor La[O1-xFx]FeAs (x = 0.05−0.12) with Tc = 26 K*. Chem. Soc, 160, (2008) 3296.
Doi: https://www.doi.org/10.1021/ja800073

[4] I.R. Shein, A.L. Ivanovskii, *Elastic, electronic properties and intra-atomic bonding in orthorhombicand tetragonal polymorphs of BaZn2As2 from first-principles calculations*, Journal of Alloys and Compounds 583 , (2014) 100–105.
Doi: https://www.doi.org/10.1016/j.jallcom.2013.08.118

[5] I. Zutic, J. Fabian, S. Das Sarma, *Spintronics: Fundamentals and applications*, Rev. Mod. Phys. 76, (2004) 323.
Doi: https://www.doi.org/10.1103/RevModPhys.76.323

[6] H. Katayama-Yoshida, K. Sato, T. Fukushima, M. Toyoda, H. Kizaki, V.A. Dinh,P.H. Dederichs, *Theory of ferromagnetic semiconductors*,Phys. Stat. Sol. (a) 204, (2007) 15.
Doi: https://www.doi.org/10.1103/PhysRevB.59.9818

[7] A. L .Ivanovskii , *Magnetic effects induced by sp impurities and defects in nonmagnetic sp materials*, Phys.-Usp. 50, (2007) 1031.
Doi: https://www.doi.org/10.1002/pssr.201206411

[8] T. Dietl, *A ten-year perspective on dilute magnetic semiconductors and oxides*, Nature Mater. 9, (2010) 965.
Doi: https://www.doi.org/10.1038/nmat2898

[9].Bardeen. J, Cooper. N. L, Scherieffer, *Theory of dirty superconductors*, Phys. Rev. 108. (1957) 1175.
Doi: https://www.doi.org/10.1016/0022-3697(59)90036-8

[10] Y. Kamihara , T . Watanabe, M. Hirano, H. Hosono," *Iron-Based Layered Superconductor: LaOFe* J. Am Chem. Soc., 130,11,(2008) 3296_ 3297.
Doi: https://www.doi.org/10.1021/ja063355c

[11] J.H. Tapp, Z.J. Tang, B. Lv, K. Sasmal, B. Lorenz, P.C.W. Chu, A.M. Guloy,LiFeAs: *An intrinsic FeAs-based superconductor with Tc=18 K*. Phys. Rev. B 78, (2008) 060505.
Doi: https://www.doi.org/10.1103/PhysRevB.78.060505

[12] Q. Huang, Y. Qiu, W. Bao, M.A. Green, J.W. Lynn, Y.C. Gasparovic, T. Wu, G. Wu, X.H. Chen, Neutron-diffraction measurements of magnetic order and a structural transition in the parent BaFe2As2 compound of FeAs-based high-temperature superconductors, Phys. Rev. Lett 101 (2008) 257003.
Doi: https://doi.org/10.1103/PhysRevLett.101.257003

[13] X. H .Chen, T .Wu, G. Wu, R .H. L iu, H .Chen, D .F. Fang, *Superconductivity at 43 K in SmFeAsO1-xF x Nature* 453(7196) , (2008) 761-762.
Doi: https://www.doi.org/10.1038/nature07045

[14] G .F. Chen, Z.Li, D.Wu, G.Li, W.Z.Hu, J.Donng, P.Zheng,J.L.Luo, N.L.Wang , *Superconductivity at 41 K and its competition with spin-density-wave instability inlayered CeO1−xFxFeAs* Phys. Rev. Lett. 100 (2008) 247002. Doi: https://www.doi.org/10.1103/PhysRevLett.100.247002

[15] W. Kohn, A.D. Becke, R.G. Parr, *Density functional theory of electronic structure*, J. Phys. Chem. 100 (31) ,(1996) 12974–12980.
Doi: https://www.doi.org/10.1021/jp960669l

[16] W. Kohn, L.J. Sham, *Self-consistent equations including exchange and correlation effects*, Phys. Rev. 140 (4A) ,(1965) A1133.
Doi: https://www.doi.org/10.1103/PhysRev.140.A1133

[17] P. Blaha, K. Schwarz, P. Sorantin, S. Trickey, *Full-potential, linearized augmented plane wave programs for crystalline systems*, Comput. Phys. Commun. 59 (2) (1990) 399–415.
Doi: https://doi.org/10.1016/0010-4655(90)90187-6

[18] P. Blaha, K. Schwarz, G. Madsen, D. Kvasnicka, J. Luitz, , *An augmented plane wave+ local orbitals program for calculating crystal properties*. Phys. Rev. B 64, (2001) 195134.
Doi: https://www.doi.org/10.1103/PhysRevB.64.195134

[19] J.P. Perdew, K. Burke, M. Ernzerhof, G*eneralized gradient approximation made simple*, Phys. Rev. Lett. 77, (1996) 3865.
Doi: https://www.doi.org/10.1007/s40089-020-00311-z

[20] A. Rajabpour, L. Seidabadi, M. Soltanpour, *Calculating the Bulk Modulus of Iron and Steel Using Equilibrium Molecular Dynamics Simulation, Procedia Materials* Science 11, (2015) 391 – 396
Doi: https://www.doi.org/10.1016/j.mspro.2015.11.005

[21] N. Amani, M. Hantehzadeh, H. Akbari, A. Boochani, Electronic, *optical and thermoelectric properties of the WS2–GaN interfaces: a DFT study,*International Nano Lettersvolume 10, (2020) 249–261.
Doi: https://www.doi.org/10.1007/s40089-020-00311-z

[22] S. Lemal, F. Ricci, D. I. Bilc, M.J. Verstraete, P.Ghosez, *Magnetic instabilities in doped Fe2YZ full-Heusler thermoelectric compound*s, Physics Review B 100, (2019) 161201.
Doi: https://www.doi.org/10.3390/nano2040379

[23] S. D. Guo, L. Qiu, *Thermoelectric properties of topological insulator BaSn2*, J. Phys. D Appl. Phys. 50, (2017) 015101.
Doi: http://www.iopscience.iop.org/0022-3727.

[24] D.K. Ko, Y.J. Keng, C.B. Murray, *Enhanced thermopower via carrier energy filtering in solution-processablePt–Sb2Te3 nanocomposites*, Nano Lett. 11, (2011) 2841.
Doi: https://www.doi.org/10.1016/0022-3697(59)90036-8

[25] L. Muchler, F. Casper, B. Yan, S. Chadov, C. *Felser, Frontispiece, topological insulators and thermoelectric materials*, Phys. Status Solidi RRL 7, (2013) 91–100.
Doi: https://www.doi.org/10.1002/pssr.201206411

[26] Y.V. Ivanov, A.T. Burkov, D.A. Pshenay-Severin, *Thermoelectri properties of topological insulators*, Phys. Status Solidi B 255.7, (2018) 1800020.
Doi: https://www.doi.org/10.1002/pssb.201800020

[27] Hai-Long Sunet Al, *Remarkably High Thermoelectric Efficiencies of the Half-HeuslerCompounds BXGa (X = Be, Mg, and Ca)*, ACS Appl. Mater. Interfaces 12 (2020) 5838−584.
Doi: https://www.doi.org/10.1021/acsami.9b19198

[28] Q. Y. Xue, H. J.Liu, D. D. Fan, ,L. Cheng, B. Y. Zhao, J. Shi . LaPtSb, *A Half-Heusler Compound with High Thermoelectric Performance*. Phys. Chem. Chem. Phys. 18 (2016) 17912−17916.
Doi: https://www.doi.org/10.1134/S1063784209090254

[29] M. Hong, T.Wang, T.Feng, Q.Sun, Xu. SMatsumura, S.Pantelides, S. T. Zou, J,Chen, Z.-G, *Strong Phonon-Phonon Interactions Securing Extraordinary Thermoelectric Ge 1-x SbxTe with Zn-Alloying-Induced Band Alignment*. J. Am. Chem. Soc. 141, (2019) 1742−1748.
Doi: https://www.doi.org/10.1021/jacs.8b12624

[30] D. LI. Guo, C. Li, K. Shao, B.Chen, D. Ma, Y. Sun, J. Zeng, W, *The Anisotropic Thermoelectricity Property of AgBi3S5 by First- Principles Study*. J. Alloys Comp.773, (2019) 812−818.
Doi: https://www.doi.org/10.1016/j.jallcom.2018.09.336

[31] Z. J. Yang, T.J. Antosiewicz, T. Shegai, Role of materia *Role of material loss and mode volume of plasmonic nanocavities for strong plasmon-exciton interactions.* Phys. 24, 18, (2016) 20373-20381.
Doi: https://www.doi.org/10.1364/OE.24.020373

[32] R. yahyazadeh, Z. Hashempour, *Effect of Hydrostatic Pressure on Optical Absorption*, 6(2), (2021) 1-22.
http://journals.miau.ac.ir/article_4768.html

[33] S. Damizadeh, M. Nayeri, F.Kalantari Fotooh, S. Fotoohi, *Electronic and Optical Properties of SnGe and SnC Nanoribbons: Electronic and Optical Properties of SnGe and SnC Nanoribbons: A First-Principles Study*, 5(4), (2020) 67-76.
http://jopn.miau.ac.ir/article_4507.html

[34] M.Saberi Lamraski,S. Babaee, S.M.Pourmortazavi, *Study of Optical Properties, Thermal Kinetic Decomposition and Stability of Coated PETN-Litholrubine nano-Composite via Solvent/None-Solvent Method Using Taguchi Experimental Design, 4, (* 2019) 11-15.
http://journals.miau.ac.ir/article_3759.html

[35] S. J. Mousavi, *First–Principle Calculation of the Electronic and Optical Properties of Nanolayered ZnO Polymorphs by PBE and mBJ Density Functionals Received*. 2(4),(2017) 1-18.
http://jopn.miau.ac.ir/article_2570.html

[36] M.R. Mohebbifar, M. Zohrabi, *Influence of Grating Parameters on the Field Enhancement of an Optical Antenna under Laser Irradiation*, 4(4) (2019) 65-80.
http://jopn.miau.ac.ir/article_3758.html